THE JOURNAL OF PHYSICAL CHEMISTRY B
A JOURNAL OF THE AMERICAN CHEMICAL SOCIETY

pubs.acs.org/JPCB

Article

Simulation of the Chiral Sum Frequency Generation Response of Supramolecular Structures Requires Vibrational Couplings

Daniel Konstantinovsky, Ethan A. Perets, Elsa C. Y. Yan,* and Sharon Hammes-Schiffer*

Cite This: *J. Phys. Chem. B* 2021, 125, 12072–12081

Read Online

ACCESS | Metrics & More | Article Recommendations | Supporting Information

ABSTRACT: Chiral vibrational sum frequency generation (SFG) spectroscopy probes the structure of the solvation shell around chiral macromolecules. The dominant theoretical framework for understanding the origin of chiral SFG signals is based on the analysis of molecular symmetry, which assumes no interaction between molecules. However, water contains strong intermolecular interactions that significantly affect its properties. Here, the role of intermolecular vibrational coupling in the chiral SFG response of the O−H stretch of water surrounding an antiparallel β-sheet at the vacuum−water interface is investigated. Both intramolecular and intermolecular couplings between O−H groups are required to simulate the full lineshape of the chiral SFG signal. This dependence is also observed for a chiral water dimer, illustrating that this phenomenon is not specific to larger systems. We also find that a dimer of C_{3v} molecules predicted to be chirally SFG-inactive by the symmetry-based theory can generate a chiral SFG signal when intermolecular couplings are considered, suggesting that even highly symmetric solvent molecules may produce chiral SFG signals when interacting with a chiral solute. The consideration of intermolecular couplings extends the prevailing theory of the chiral SFG response to structures larger than individual molecules and provides guidelines for future modeling.

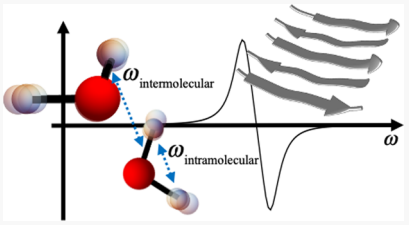

INTRODUCTION

Biological processes occur in aqueous solution or at an interface involving water, and this water does not always behave as a passive medium. In particular, water molecules can bind to biomacromolecules and modulate their structure and function. These water molecules can interact with a solute tightly enough to adopt a large-scale structure but loosely enough to form a structural ensemble and exchange rapidly with the bulk solvent. A complete understanding of the behavior of biomacromolecules requires a thorough description of these water molecules. Chiral vibrational sum frequency generation (SFG) spectroscopy is an emergent technique to probe the solvation shell of biomacromolecules.[1−3] As a second-order nonlinear chirality-sensitive technique, chiral SFG can suppress background signals from water in non-centrosymmetric interfacial environments and isotropic bulk water. Thus, it can selectively detect solvent molecules forming chiral supramolecular structures around chiral macromolecules, such as DNA and proteins.[1,2] Vibrational spectroscopy can resolve subpopulation exchange on the picosecond timescale and does not require molecular labels that perturb chemical structures. Importantly, chiral SFG can detect chiral solvent structures formed by interactions with biomacromolecules even if the individual solvent molecules in that structure exchange rapidly.[1,2,4,5]

The last two decades have seen extensive applications of chiral SFG in biological systems.[6−8] In 2003, a chiral SFG spectrum of the amide I response of a protein at the air−water interface was published.[7] Our group extended the application to probe various protein secondary structures using the amide I, C−H, and N−H stretch modes.[6,9,10] Achiral spectra of DNA in the O−D and C−H stretch regions showed that SFG can detect the effects of solvation in D_2O.[11] Chiral SFG spectra of the C−H stretch in DNA were reported.[12,13] Others have applied femtosecond time-resolved SFG to monitor the relaxation of the amide I vibrational mode in the presence of a water solvent.[14] Reports of the chiral SFG response of water surrounding DNA and an antiparallel β-sheet protein demonstrated that even highly dynamic solvation structures of a biological system can be probed with SFG.[1,2,5] We recently used the internal heterodyne phase-sensitive chiral SFG method[15] and observed that the phase of the water O−H stretching bands is correlated with the absolute handedness of (L-) and (D-) proteins, further establishing a method for probing the hydration structures of biomacromolecules.[5]

Simpson's chiral SFG theory[16] has served as a foundation for predicting and interpreting chiral SFG studies of interfaces. This theory takes intramolecular couplings into account by considering molecular units larger than single bonds when assigning the symmetry of vibrational modes.[16] Because this symmetry-based theory has been derived and applied mainly for chiral macromolecules (e.g., various protein secondary

Received: July 16, 2021
Revised: October 5, 2021
Published: October 26, 2021

structures), intermolecular coupling is not relevant and thus not considered. However, the hydrogen-bonding interactions between water molecules are paramount. Thus, the recent reports of chiral SFG signals from the water solvent surrounding biomacromolecules[1,2,5] call for examination of intermolecular couplings.

In this study, we examine the impact of intermolecular coupling as well as intramolecular coupling on chiral SFG signals[16] using an electric field mapping method.[17−19] We show that intramolecular or intermolecular vibrational coupling is necessary to produce nonzero chiral SFG signals in the simulation and that the signal intensity contributed by these two couplings is comparable. In contrast, neither of these couplings is needed to generate an achiral SFG response, and the achiral SFG response is only mildly affected when such couplings are included. We demonstrate these effects using the antiparallel β-sheet system formed by the LK$_7\beta$ (LKLKLKL) peptide at the vacuum−water interface (Figure 1).[20] To examine the fundamental origin of the coupling effect, we also study a small model system composed of a dimer of water frozen in a chiral configuration. We find that couplings are necessary to observe a chiral SFG signal in this minimal system as well. Similarly, we examine a dimer of ammonia with the C_{3v} symmetry in contrast to the C_{2v} symmetry of water to further illustrate the interplay of molecular symmetry and vibrational couplings for generating chiral SFG responses. Finally, we examine a dimer of methane to show that the trends seen with the ammonia system translate to other highly symmetric point groups. We discuss our results in the context of Simpson's symmetry-based theory.[16]

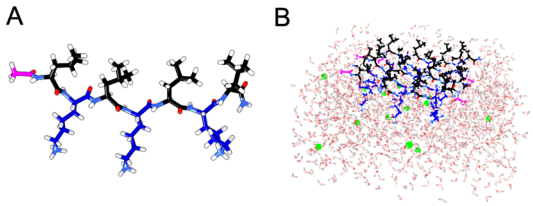

Figure 1. The LK$_7\beta$ (LKLKLKL) peptide model system. (A) Each LK$_7\beta$ peptide consists of alternating leucine (black) and lysine (blue) residues and is capped with an acetyl group (magenta) on the N-terminus and an NH_2 group on the C-terminus. (B) An antiparallel β-sheet is constructed at the vacuum−water interface from five LK$_7\beta$ peptides arranged such that leucine side chains point toward the vacuum and lysine side chains point into the water. The system is neutralized with Cl^- ions (green). Approximately 1350 water molecules surround the peptide. The simulation box is roughly 45 × 45 × 45 Å. Half of the box is composed of the system and the other half is vacuum.

This study will be helpful to experimentalists considering the SFG spectra of isotopically labeled water molecules in biological systems (e.g., HOD largely lacks intramolecular coupling but still has intermolecular coupling) and solvent systems other than water for chiral polymers and macromolecules. The results will also guide theorists in proposing approximations to the dipole-polarizability time correlation function formalism[21] for calculating SFG responses. In particular, although couplings can be omitted to save computational time for calculating achiral SFG spectra, they must be included to model chiral SFG responses.[22] We recognize that couplings have not always been reported to be essential for a chiral SFG signal.[23] We discuss the intermolecular and intramolecular couplings in these previous studies in the context of our findings in the Discussion Section.

SYMMETRY-BASED CHIRAL SFG THEORY

We interpret the simulated SFG spectra of water in this study based on Simpson's symmetry-based chiral SFG theory.[16] Herein, (x, y, z) represents the laboratory frame coordinates, and (a, b, c) represents the molecular frame coordinates. The indices I, J, and K are used to indicate x, y, or z, whereas the indices i, j, and k are used to indicate a, b, or c.

Chiral SFG signals can be generated from a chiral interface, which is defined as a molecular system with C_∞ symmetry with the rotational axis aligned with the surface normal. Within the electric dipole approximation, SFG signals arise from the second-order nonlinear response of materials

$$\boldsymbol{P} = \boldsymbol{P}_0 + \chi^{(1)}\boldsymbol{E}_1 + \chi^{(2)}\boldsymbol{E}_1\boldsymbol{E}_2 + \ldots \quad (1)$$

where $\boldsymbol{P}$ is the material's polarization, $\boldsymbol{E}_1$ and $\boldsymbol{E}_2$ are incident electric fields, and $\chi^{(n)}$ is the n^{th}-order susceptibility tensor.[24] In vibrational SFG, one beam is in the mid-infrared (IR) range and the other is in the visible range but typically far from electronic resonance.[25−27] The $\chi^{(2)}$ tensor contains 27 elements with $\chi^{(2)}_{IJK}$ as in

$$E^I_{\text{SFG}} \propto \sum_{JK} \chi^{(2)}_{IJK} E^J_{\text{vis}} E^K_{\text{IR}} \quad (2)$$

where E^I_{SFG}, E^J_{vis}, and $E^K_{\text{IR}}$are the optical fields of the SFG, visible, and IR beams, respectively, with the indices I, J, and K specifying the components of these optical fields along the Cartesian direction (x, y, or z) in the laboratory reference frame (Figure 2). Manipulating the polarization of the IR and visible beams and the detector of the SFG signal isolates different elements of the $\chi^{(2)}$ tensor. Among the 27 elements, those with all three indices that are different ($I \neq J \neq K$) are called orthogonal. Orthogonal $\chi^{(2)}$ elements for a uniaxial assembly can be nonzero only for a chiral interface.

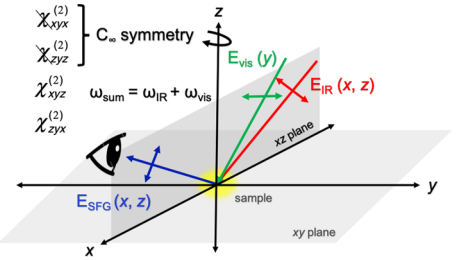

Figure 2. Schematic depiction of a vibrational SFG experiment with the *psp* polarization setting, where *p* indicates polarization on the plane of incidence (the *xz* plane) and *s* indicates polarization perpendicular to that plane (i.e., along the *y* plane). The polarization is specified in the order of sum frequency (detector), visible, and IR. The *psp* polarization setting isolates four elements of the second-order susceptibility tensor ($\chi^{(2)}$). Among these four elements, $\chi^{(2)}_{xyx} = \chi^{(2)}_{zyz} = 0$ due to the C_∞ symmetry of a noncentrosymmetric interface (*xy* plane) about the *z*-axis and $\chi^{(2)}_{xyz} = 0$ given the symmetry of the Raman polarizability tensor in the absence of electronic resonance. Ignoring Fresnel factors, the chiral response is given by $\chi^{(2)}_{psp} \propto \chi^{(2)}_{zyx}$.

To perform a chiral SFG experiment, the *psp* polarization setup can be used (Figure 2), where *s* polarization lies along the *y*-axis, and *p* polarization lies along the *x*- and *z*-axes on the plane of incidence. Figure 2 shows that the effective second-order susceptibility, $\chi^{(2)}_{psp}$, depends only on $\chi^{(2)}_{xyx}$, $\chi^{(2)}_{zyz}$, $\chi^{(2)}_{xyz}$, and

https://doi.org/10.1021/acs.jpcb.1c06360
J. Phys. Chem. B 2021, 125, 12072−12081

$\chi^{(2)}_{zyx}$. The first two elements vanish due to isotropy in the *xy* plane, as is found at a noncentrosymmetric interface.[16] The last two elements are orthogonal and $\chi^{(2)}_{xyz} = 0$ under the condition of electronic nonresonance due to the symmetric polarizability tensor.[6,16] Hence, the experimental measurable, $\chi^{(2)}_{psp}$, is only related to $\chi^{(2)}_{zyx}$:

$$\chi^{(2)}_{psp} \propto \chi^{(2)}_{zyx} - \chi^{(2)}_{xyz} = \chi^{(2)}_{zyx} \tag{3}$$

In the symmetry-based theory, the system of interest has C_∞ symmetry. Although this is true for many experimental systems, it is not true for molecular dynamics (MD) trajectories with limited sampling. To avoid this issue, the $\chi^{(2)}_{xyz}$ term in eq 3 is kept in our calculations for extracting chiral SFG signals from MD trajectories (see eqs 9 and 10 and S4). The current study assumes a *psp* setup, but the methods and results are directly applicable to the other two polarization setups (*spp* and *pps*) for chiral SFG experiments.

The macroscopic chiral SFG response, $\chi^{(2)}_{psp}$, is the ensemble average of microscopic responses given by molecular hyperpolarizabilities (β).[26] The hyperpolarizability arises from the transition dipole and polarizability derivatives as in

$$\beta_{ijk} \propto \left(\frac{\partial \alpha_{ij}}{\partial Q}\right)\left(\frac{\partial \mu_k}{\partial Q}\right) \tag{4}$$

where $\boldsymbol{\alpha}$ is the transition polarizability matrix, $\boldsymbol{\mu}$ is the transition dipole vector, and Q is a normal mode coordinate. The ensemble average can be expressed as

$$\chi^{(2)}_{IJK} \propto \sum_{i,j,k} \langle R_{Ii}(\psi) R_{Jj}(\theta) R_{Kk}(\phi)\rangle \beta_{ijk} \tag{5}$$

where $\boldsymbol{R}$ is an Euler rotation matrix, ϕ, θ, and ψ are Euler rotation angles, (*i*, *j*, *k*) represents the molecular frame, (*I*, *J*, *K*) represents the laboratory frame, and the brackets indicate averaging over molecular orientations. Applying eq 5 and integrating over all rotations in the *xy* plane (ϕ) leads to

$$\begin{aligned}\chi^{(2)}_{zyx} \propto \frac{1}{2}\{&(-\beta_{cab} + \beta_{cba})\cos^2(\theta) + \cos(\theta)\\ &\sin(\theta)[(\beta_{aab} - \beta_{aba} + \beta_{cbc} - \beta_{ccb})\cos(\psi)\\ &+ (-\beta_{bab} + \beta_{bba} + \beta_{cac} - \beta_{cca})\sin(\psi)]\\ &+ \sin^2(\theta)((-\beta_{abc} + \beta_{acb})\cos^2(\psi)\\ &- (\beta_{aac} - \beta_{aca} - \beta_{bbc} + \beta_{bcb})\cos(\psi)\sin(\psi)\\ &+ (\beta_{bac} - \beta_{bca})\sin^2(\psi))\}\end{aligned} \tag{6}$$

The *c*-axis points along the primary rotation axis of the molecule. Although all chiral molecular β_{ijk} ($i \neq j \neq k$) elements are zero for water molecules with C_{2v} symmetry, the achiral β elements can combine to give rise to chiral $\chi^{(2)}$ elements if the water molecules are arranged in a chiral configuration at the interface. Eliminating all zero-valued β elements in eq 6[16,28] based on symmetry arguments results in the expression of the chiral $\chi^{(2)}_{zyx}$ element as

$$\chi^{(2)}_{zyx} \propto \frac{1}{4}\sin^2(\theta)\sin(2\psi)(\beta_{aac} - \beta_{bbc} + \beta_{bcb} - \beta_{aca}) \tag{7}$$

Therefore, chiral SFG can be sensitive to water when the water molecules adopt a chiral supramolecular structure in the solvation shells of biomacromolecules (e.g., proteins and DNA) at interfaces. We are not the first to notice this possibility. Simpson theorized the appearance of chiral spectra from achiral chromophores with certain symmetries as early as 2004,[16] and in 2012, Laaser and Zanni published a theory of chiral 2D-SFG signals arising from pairs of achiral but coupled chromophores.[29]

Derivation of eq 7 from eq 6 suggests that water is quite a unique solvent with respect to generating a chiral SFG response. Its C_{2v} symmetry is high enough (with two reflection planes) to eliminate all microscopic chiral (orthogonal) β elements but low enough to preserve some achiral β elements that can still contribute to the macroscopic chiral $\chi^{(2)}_{zyx}$, as shown in eq 7. Hence, the symmetry-based theory predicts that chiral supramolecular assemblies of water situated in an interfacial environment with C_∞ symmetry are chirally SFG-active. However, when the molecule becomes just slightly more symmetric (such as C_{3v}), the prediction can be drastically different because the higher the symmetry, the more β elements become zero. In particular, all β elements in eq 6 are zero or cancel out for a C_{3v} molecular system. Thus, the symmetry-based theory predicts that a C_{3v} molecule (e.g., ammonia, NH_3) cannot generate chiral signals (e.g., N−H stretching in NH_3) even when the molecules are assembled into chiral supramolecular structures at an interface.[16,28] Below, we will discuss how introducing intermolecular vibrational couplings can alter this prediction, leading to a chiral SFG response in simulated spectra.

COMPUTATIONAL METHODS

MD Simulations. A starting structure of five antiparallel $LK_7\beta$ (LKLKLKL) strands (Figure 1A) was placed into a box with at least 10 Å of TIP4P-Ew water (a modification of the original TIP4P model that is optimized for Ewald summation treatment of long-range interactions)[23] next to each of the four edges of the protein and above and below it.[5] Half of the water was removed and Cl^- ions were added to the aqueous half to neutralize the system, creating a vacuum above the neutral solvated protein system.[2,5,30] The protein was placed at the interface with the lysine side chains pointing into the water and the leucine side chains facing the vacuum (Figure 1B) and was modeled with the AMBER ff14SB force field.[31] The N-termini were acetylated, and the C-termini were amidated ($-NH_2$). The energy of the system was minimized followed by equilibration in an *NVT* (constant number of particles, volume, and temperature) ensemble for 6 ns at 298 K. Langevin dynamics was propagated with a friction coefficient of 1 ps^{-1} and a timestep of 1 fs. Long-range electrostatic interactions were treated with the particle mesh Ewald method.[32] Water molecules were kept rigid with the SETTLE algorithm, and bonds involving protein hydrogens were constrained with the SHAKE method.[33,34] Configurations were saved every 10 fs. For the calculation of achiral SFG spectra, trajectories were wrapped in the *z*-direction to consolidate the slab into a single unit, and spectral calculations took periodic boundary conditions in the *x*- and *y*-directions into account. Wrapping was not necessary for chiral SFG calculations (see Supporting Information for explanation). The simulations were performed with the OpenMM 7.4 library on a Tesla V100 GPU using CUDA 9.2.[35] See the Supporting Information for full equilibration details.

SFG Calculations of the Aqueous Protein System. The chiral SFG response was calculated using the dipole-polarizability time correlation function approach with electric field mappings.[17−19,21,36] This approach uses empirical mappings

https://doi.org/10.1021/acs.jpcb.1c06360
J. Phys. Chem. B 2021, 125, 12072−12081

between the electric field measured at the water hydrogens in the direction along the O−H bond and quantities such as the dipole derivative, vibrational frequency, and vibrational couplings. The inhomogeneous limit approximation was used as given in the expression

$$\chi^{(2)}_{IJK}(\omega) \approx \left\langle \sum_{a=1}^{N_{OH}} \frac{\sum_{b=1}^{N_{OH}} \alpha^{b}_{IJ} U_{ba} \sum_{b=1}^{N_{OH}} \mu^{b}_{K} U_{ba}}{\lambda_a - \omega - \frac{i}{2\tau}} \right\rangle \tag{8}$$

where $\boldsymbol{\alpha}$ is the transition polarizability tensor of each O−H bond computed with a bond-polarizability approach, $\boldsymbol{\mu}$ is the O−H stretch transition dipole moment, $\boldsymbol{U}$ is the eigenvector matrix of the array of vibrational frequencies and couplings, λ is the corresponding set of eigenvalues of the Hamiltonian matrix, and τ is the vibrational lifetime, which is assumed to be 1.3 ps.[17,18,37] The indices a and b refer to particular O−H bonds, while the indices I, J, and K each refer to the dimensions x, y, z making up a component of $\chi^{(2)}$.

In the inhomogeneous limit, the response is a simple average over conformations with no explicit time dependence.[17] This approach was used to maximize the number of frames averaged during the procedure for an optimal signal-to-noise ratio. The computationally less expensive alternative, the time-averaging approximation, correlates the dipole and polarizability across a short time interval with the frequencies and couplings averaged over that interval. As shown in Figure S1, this approach did not significantly change the spectrum other than increasing the noise.[17] A fully time-dependent correlation function approach such as that introduced previously[19] is not feasible for a system of this size and a signal that requires long trajectories to converge.

The calculation of intermolecular couplings using this approach requires a dipole−dipole distance. To find this distance, each O−H bond was assigned an effective dipole location 0.67 Å from the oxygen along the bond.[19] For achiral SFG, the contribution of the bottom half of the system was suppressed with a sigmoidal damping function to avoid contributions from a second surface opposite the surface containing the protein.[19] The z-component of the effective dipole location of each O−H bond was used to assign the bond's position along the z-axis for the damping function. No damping was necessary for chiral SFG calculations because the protein stayed on the top surface.

The polarizability is assumed to be localized at each O−H bond, and the ratio of the component of the polarizability derivative along the bond to the components perpendicular to the bond is assumed to be constant.[36,38] We use a ratio of 5.6, as used by the Skinner group in the past.[36] The value of this constant affects the magnitude and sign of the chiral SFG response but does not affect the position of the peaks (see Supporting Information, Figure S2).

For each SFG calculation, 100 ns of MD data was analyzed, corresponding to 10,000,000 frames. The electric fields needed for the frequency mapping were calculated using the previously optimized charges for the atoms of TIP4P water,[19] while AMBER ff14sb charges were used for the protein and ions.[19,31] The protein was assumed not to have any vibrational coupling with water molecules and therefore influenced the system only geometrically and as a source of electric field. The frequency resolution was 1 cm^{-1}. The calculations were implemented in Python and Cython using the MDAnalysis and NumPy libraries.[39,40]

Extracting Chiral SFG Signals from MD Trajectories. The chiral SFG theory is derived based on the assumption that the system of interest has C_∞ symmetry. This is not true for MD trajectories with limited sampling. However, it is not necessary to sample every orientation equally.[23] Instead, one can simply assume that each frame of the trajectory is rotated by a random angle about the z-axis, and then integrate over all values of the angle. In the rotated frame of reference denoted by the prime symbol, each component of $\chi^{(2)}$ is transformed according to

$$\begin{aligned} \chi^{(2)}_{z'y'x'} &\rightarrow \chi^{(2)}_{zyx} - \chi^{(2)}_{zxy} \\ \chi^{(2)}_{x'y'z'} &\rightarrow \chi^{(2)}_{xyz} - \chi^{(2)}_{yxz} \end{aligned} \tag{9}$$

and therefore, according to eq 3, the *psp* response is given by

$$\chi^{(2)}_{psp} \propto \chi^{(2)}_{zyx} - \chi^{(2)}_{zxy} + \chi^{(2)}_{yxz} - \chi^{(2)}_{xyz} \tag{10}$$

where $\chi^{(2)}_{yxz} - \chi^{(2)}_{xyz}$ in the original frame, which comes from $\chi^{(2)}_{x'y'z'}$, is approximately equal to zero because the Raman polarizability tensor, which corresponds to the first two indices in $\chi^{(2)}$, is approximately symmetric when the incident beam frequencies are far from electronic resonance.[23] This leaves

$$\chi^{(2)}_{psp} \propto \chi^{(2)}_{zyx} - \chi^{(2)}_{zxy} \tag{11}$$

SFG Calculation of Model Systems. To calculate the SFG spectra of the model systems, the approach described above (eq 8) was adapted and implemented in a Mathematica notebook. Unlike our SFG calculations of the protein system, electric fields were ignored in the model system calculations, and the gas-phase values of mapped quantities for the O−H bond were used for all systems.[36] The water dimer structure coordinates were obtained from a pair of water molecules taken from near LK-7β in a frame of an MD trajectory. The C_{3v} (i.e., ammonia) molecule was built as a perfectly trigonal pyramidal structure (109.5° between adjacent bonds), and the dimer was built using simple geometric transformations that created a segment of a chiral helix. The same procedure was used to create a dimer of methane molecules. The chiral SFG spectrum of each model structure was calculated by averaging 200 conformations by rotating around the z-axis. Here $\chi^{(2)}_{psp} = \chi^{(2)}_{zyx} - \chi^{(2)}_{xyz} + \chi^{(2)}_{zyz} - \chi^{(2)}_{xyx}$ (see Figure 2), and the disappearance of the $\chi^{(2)}_{zyz}$ and $\chi^{(2)}_{xyx}$ components was monitored to ensure adequate rotational averaging (full integration over all rotations was impractical). The negative signs arise from the vectors specifying the orientations of the incoming and outgoing beams.[23] Unless otherwise stated, the O−H/N−H/C−H groups were treated as equivalent in terms of dipole and polarizability magnitudes, intramolecular and intermolecular couplings, and vibrational resonance frequency. Natural fluctuations in these quantities were not sufficient to create a chiral SFG signal in the absence of couplings in the protein-containing system (data not shown), so variation in these quantities was not considered in the model systems. The O−H/N−H stretch frequencies were set to 3400 cm^{-1}, roughly reflecting the IR spectra of the O−H and N−H stretches, while the C−H frequency of methane was set to 2900, roughly reflecting the IR spectra of liquid alkanes.[36,41] Note that the precise value of the resonance frequency does not affect the predicted spectra except by shifting them (see Figure S3). The vibrational lifetime (i.e., Lorentzian damping coefficient) was set to 0.01 s for the simple model dimer systems to achieve a

https://doi.org/10.1021/acs.jpcb.1c06360
J. Phys. Chem. B 2021, 125, 12072−12081

Lorentzian peak broadness similar to that observed in the real system. If the lifetime is assumed to be in a more realistic range (~1 ps), the peaks become extremely sharp and less convenient to plot. The conclusions presented here are not affected by the choice of damping coefficient. The frequency resolution was 10 cm^{-1}. The polarizability was modeled as above with a parallel-to-perpendicular polarizability derivative ratio of 5.6 assumed for both water and ammonia.[36,42]

RESULTS

Biomacromolecules have been observed to organize surrounding water into dynamic chiral superstructures.[1,2,5,43] Here, we use a model system consisting of the antiparallel β-sheet formed by the short LK$_7\beta$ peptide that is stabilized by the vacuum−water interface (Figure 1). Switching the chirality of the protein amino acids from (L-) to (D-) causes the experimental chiral SFG response to flip.[5] This effect is clearly reproduced in our calculations (Figure 3). The chiral (*psp*)

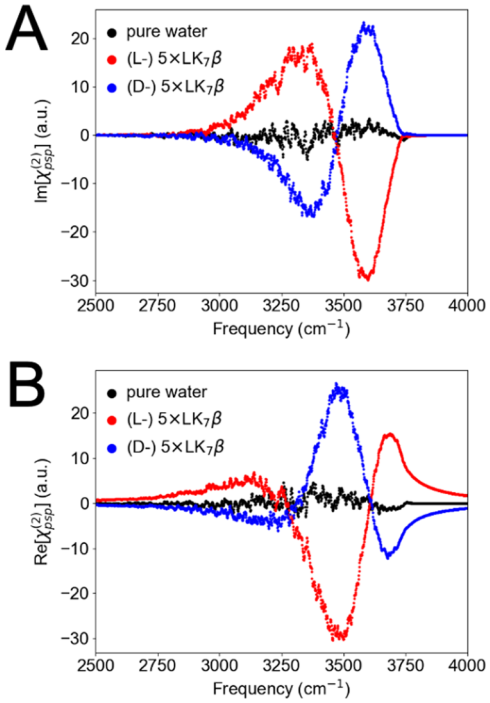

Figure 3. (A) Imaginary and (B) real components of the *psp* SFG response of the O−H stretch of water around a pentamer of (L-) LK$_7\beta$ (red) and its (D-) enantiomer (blue) at the vacuum−water interface (see Figure 1 for structure) as well as a pure water interface with the same simulation box size (black). Spectra are averaged over 10,000,000 frames from 100 ns of MD simulation. Spectra are unnormalized.

signal is around two orders of magnitude weaker than the achiral (*ssp*) signal and converges about 10 times slower (Figure S4). These observations are likely the result of the complexity and variety of the chiral water supramolecular structures, the relatively slow dynamics of the protein scaffold compared to water, and the relatively small number of water molecules actively participating in the solvation shell. An interface containing pure water produces no significant chiral SFG signal (Figure 3). The small residual signal for pure water may be due to imperfect MD sampling, which is limited by the high computational cost of the SFG spectrum calculations for systems of this size (~1350 water molecules). Figure S5 shows that two independent simulations of a pure water interface system produce extremely noisy and completely different signals, confirming that the chiral SFG response of a pure water surface is effectively zero. The small difference in intensity between (L-) and (D-) LK$_7\beta$ signals is most likely also a result of limited sampling due to the high computational cost.

Understanding the role of vibrational couplings in chiral SFG signals is important for the interpretation of experimental data. We find that neglecting both intermolecular and intramolecular vibrational couplings completely removes the chiral SFG signal from water around LK$_7\beta$ (Figure 4A), whereas the achiral SFG signal only blueshifts slightly when both couplings are absent (Figure 4B). Note that we neglect couplings only in the SFG calculation and not in the MD simulation, where all interactions specified by the force field are preserved. Although both intermolecular and intramolecular couplings contribute to the chiral signal, either one is enough to make it appear. Intermolecular couplings cause a small redshift in both the chiral and achiral SFG responses.[44] In real systems, this shift is likely caused by the vibrational delocalization of the O−H stretch over many molecules. Water molecules that interact with their neighbors have less electron density to devote to covalent bonds, which weakens the bonds and thus lowers the vibrational frequencies. In our model, the red shift is caused by the shift in the eigenspectrum of the coupling matrix due to significant off-diagonal components, thereby approximating the aforementioned physical effect. Because of the method by which these couplings were calculated, couplings between the O−H stretch and protein modes, for example, the N−H stretch in the protein backbone, were not included.[36] However, the protein still contributed to the spectrum by modulating the local electric field experienced by the water molecules.[31]

Figure 4C shows the distribution of vibrational couplings calculated from a representative frame of an MD simulation plotted against the dipole−dipole distance. The average value of the intramolecular coupling (−17 cm^{-1}) is much larger in magnitude than the average value of the intermolecular coupling (−0.025 cm^{-1}), but a few very short-distance (<3 Å) intermolecular couplings are larger in magnitude (>100 cm^{-1}) than any intramolecular coupling. The standard deviation of the intermolecular coupling magnitudes (1.1 cm^{-1}) indicates that these larger couplings are extremely rare.[36] In Figure 4D, intramolecular couplings are included fully, but intermolecular couplings are only included up to a distance cutoff. This plot reveals that most of the contribution to the spectral intensity from the intermolecular couplings arises from interaction distances within 3 Å, that is, from the immediate neighbors of each molecule.

Although we have shown that short-range interactions produce most of the chiral SFG signal, we have not addressed the length scale at which these interactions originate. It may be that the observed effect of couplings is additive and only valid for large macromolecular systems and not for smaller chiral assemblies. To test this possibility, we calculated the chiral SFG response of a minimal water dimer system in a chiral configuration at an interface with the macroscopic symmetry of C_∞ (Figure 5A). Figure 5A (top) shows a pair of the enantiomeric water dimers. For simplicity, we assumed that each O−H group has the same dipole moment and polarizability magnitude. Intramolecular couplings were calculated using gas-phase values[36] for mapped quantities such as the dipole derivative. Intermolecular couplings were

https://doi.org/10.1021/acs.jpcb.1c06360
J. Phys. Chem. B 2021, 125, 12072−12081

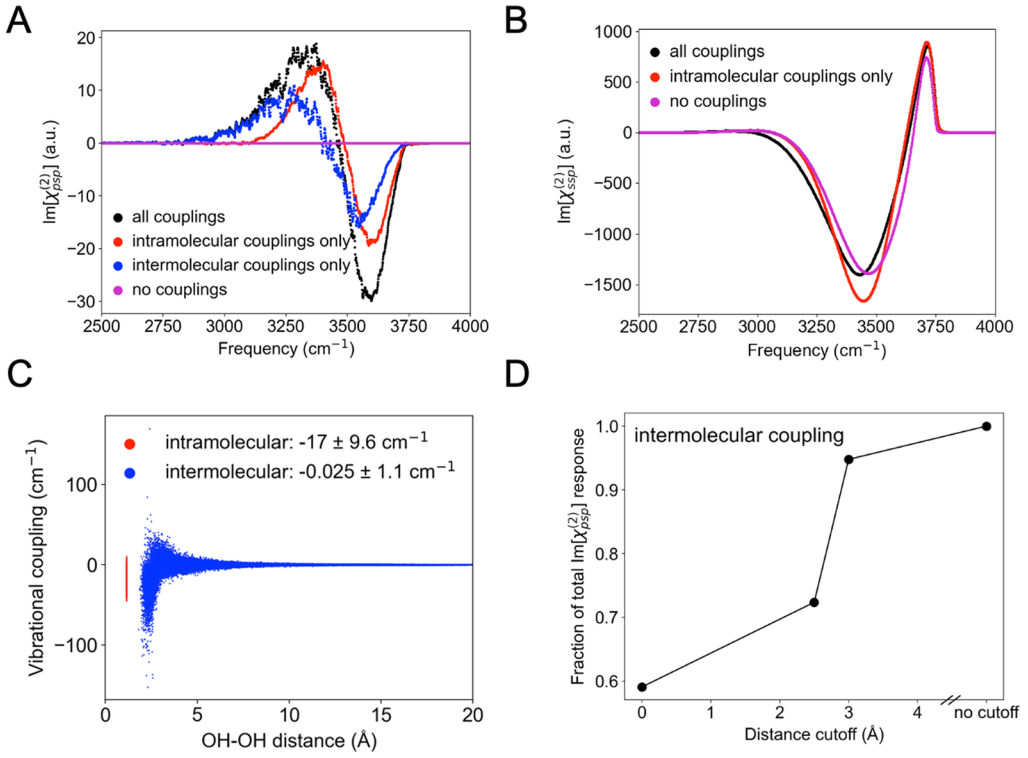

Figure 4. (A) Imaginary chiral (*psp*) SFG response of an (L-) LK$_7\beta$ pentamer at the vacuum−water interface with different treatments of O−H/O−H vibrational coupling. (B) Imaginary achiral (*ssp*) SFG response of the same (L-) LK$_7\beta$ system. (C) Intramolecular and intermolecular coupling magnitudes for the chiral SFG response between O−H groups among waters in the LK$_7\beta$ system as a function of dipole−dipole distance, where each dot represents coupling between two OH groups for one configuration obtained from an MD trajectory. The mean and standard deviation are given for each type of coupling. The intramolecular couplings (red) are given for a single distance (1.14 Å) and thus correspond to a vertical line. (D) Fraction of the total chiral SFG response (the sum of the absolute values of the responses for all frequencies) versus intermolecular coupling distance cutoff, where the distances were computed using effective dipole locations for each O−H bond.

calculated based on distance using gas-phase values for the transition dipoles, as described in the Computational Methods Section. We assumed a complex Lorentzian response with a damping factor chosen to produce peaks with a similar width as in the protein−water spectra although the peak width does not affect our conclusions. As shown in the simulated spectra (Figure 5A) from top to bottom, when all couplings are included, the mirror-image water dimers produce signals with an opposite phase. When only intramolecular couplings are considered, the intensity of the signals does not change significantly. Including just intermolecular couplings (as would be the case for a system such as HOD) produces a small but reliable signal as well. When there is no vibrational coupling, the signals disappear completely.

To further illustrate the interplay of vibrational couplings and molecular symmetry in determining the chiral SFG response, we performed the same calculation for two model systems with a high degree of symmetry: a dimer of ammonia molecules and a dimer of methane molecules, both arranged in a chiral configuration, shown as a pair of enantiomers in Figure 5B,C (top). We observed coupling effects similar to those of the water dimers but with a major difference—intramolecular couplings on their own produced no signal. This result aligns with Simpson's prediction of no chiral signal from an ideal C_{3v} or T_d (tetrahedral) molecule.[16,28] In the next section, we will discuss how intermolecular couplings can in principle break the symmetry and thereby produce chiral SFG signals in any molecule.

DISCUSSION

Water has a uniquely strong and extensive network of hydrogen bonds. These bonds significantly delocalize the O−H stretch mode and therefore change the symmetry of vibrational chromophores. To illustrate this concept, Figure 6 schematically shows how couplings change the fundamental geometry of a water dimer that is frozen in an asymmetric configuration. When O−H stretches are uncoupled, the system reduces to a set of four O−H bonds. When intramolecular couplings are added, each pair of bonds is unified, and the smallest indivisible unit of the system becomes a whole water molecule with C_{2v} symmetry. When intermolecular couplings are considered, the entire system becomes interconnected, and the fundamental geometry behind the spectral response becomes the (chiral) geometry of the entire water superstructure interacting with the chiral protein or other macromolecules.

Based on the concept that vibrational couplings change the symmetry of vibrational chromophores (Figure 6), we discuss the observations in the simulated chiral SFG spectra (Figures 4 and 5) in the context of Simpson's symmetry-based theory. First, in Figure 4A, in the case of no vibrational coupling, each O−H bond in the protein−water system is an isolated linear oscillator, and the O−H vibrational mode belongs to the $C_{\infty v}$ symmetry group. For such a system, all tensor elements of the molecular hyperpolarizability are zero except β_{ccc}, β_{aac}, and β_{bbc}, where the *c*-axis points along the O−H bond, and all three elements are either proportional or equal to each other.[28] These three elements do not contribute to the chiral $\chi^{(2)}$

https://doi.org/10.1021/acs.jpcb.1c06360
J. Phys. Chem. B 2021, 125, 12072−12081

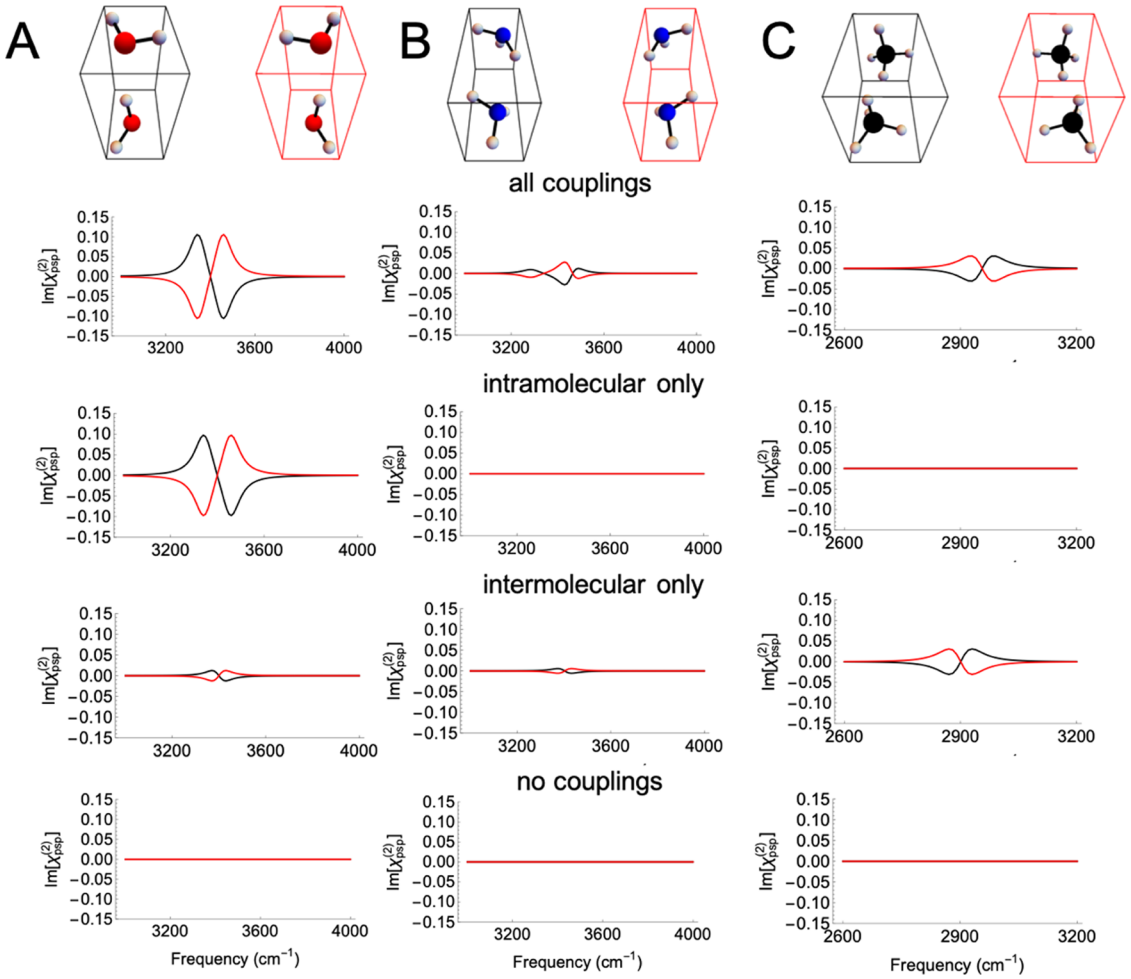

Figure 5. Effect of coupling on model dimer systems: (A) water dimer, (B) ammonia dimer, and (C) methane dimer. Top: enantiomers of the dimers. Bottom: simulated chiral SFG spectra of the dimers in mirror images (black and red) for various combinations of vibrational couplings. The peak was set at 3400 cm^{-1} for water and ammonia and at 2900 cm^{-1} for methane, and the couplings were calculated using Skinner's approach assuming no electric field, where the couplings still depend on the dipole alignment and the distance between dipoles (see Computational Methods section).

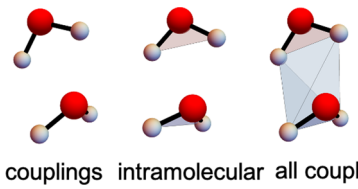

Figure 6. Schematic showing how including vibrational couplings effectively changes the geometry (and symmetry) of a molecular system.

response according to eq 6 because $\beta_{aac} = \beta_{bbc}$. Thus, chiral SFG is forbidden[16] (purple, Figure 4A). When only intramolecular couplings are considered (red, Figure 4A), the symmetry of the vibrational chromophores becomes C_{2v}. This lower symmetry leads to additional nonzero β elements (β_{aca}, β_{bcb}, β_{caa}, and β_{cbb}), where the *c*-axis is defined as the C_2 rotation axis of the molecule, which can contribute to chiral SFG as described by eq 7. Thus, the chiral SFG signal can be nonzero (red, Figure 4A). In the case of intermolecular couplings alone, each O−H group of individual water molecules communicates with O−H groups of other water molecules. This crosstalk further reduces the symmetry and results in additional nonzero β elements if the solvent surrounds a chiral template. In the extreme case, the symmetry is reduced to C_1 (with no symmetry elements) and thereby all β hyperpolarizability tensor elements are nonzero. In this case, β is associated with the delocalized vibrational chromophore due to intermolecular coupling, not individual molecules, such that β effectively becomes $\chi^{(2)}$ if the molecular frame is chosen to align with the laboratory frame. We note that β refers to the hyperpolarizability tensor of the smallest independent molecular unit of the system, which is larger than a single molecule if all couplings are considered. As long as not all β elements in eq 6 are zero or cancel out, $\chi^{(2)}_{zyx}$ does not vanish. Hence, chiral SFG is allowed (blue, Figure 4A). Finally, when both intramolecular and intermolecular couplings contribute, the net effect is a combination of the second and third cases, yielding larger chiral SFG signals (black, Figure 4A). We emphasize that both types of coupling are necessary to obtain the full lineshape although we cannot generally predict the ratio of intramolecular versus intermolecular contributions in all systems.

The above arguments can also be applied to elucidate the simulated achiral spectra shown in Figure 4B, where the signals do not significantly depend on vibrational coupling. For achiral SFG experiments performed using the *ssp* polarization

https://doi.org/10.1021/acs.jpcb.1c06360
J. Phys. Chem. B 2021, 125, 12072−12081

response, the effective $\chi^{(2)}_{ssp}$ arises from $\chi^{(2)}_{xxz}$ and $\chi^{(2)}_{yyz}$ according to the definition of coordinates presented in Figure 2, where $\chi^{(2)}_{xxz} = \chi^{(2)}_{yyz}$ due to isotropy in the xy plane. Thus, $\chi^{(2)}_{ssp}$ can be expressed in terms of β elements as in eq S11 that contains β_{ccc}. This element does not vanish even for linear structures when β is averaged over all rotations about the z-axis.[28] Hence, in the case of no couplings, where the vibrational chromophore has the $C_{\infty v}$ symmetry, the nonzero element β_{ccc} can contribute to the achiral signal (purple, Figure 4B). When intramolecular and/or intermolecular couplings are considered, the vibrational chromophores have less symmetry, which leads to more nonzero β elements that can contribute to $\chi^{(2)}_{ssp}$ as described in eq S11.

The differing sensitivity to couplings between chiral responses (Figure 4A) and achiral responses (Figure 4B) may also be due to the fundamentally different origins of the signals. Achiral signals are related to the magnitude of the z-component of the total system dipole, resolved by vibrational frequency, while chiral responses result from imperfect cancellation of hyperpolarizability terms and have no direct dependence on the overall dipole. Hence, the achiral SFG signal intensity does not depend strongly on couplings or any other symmetry-breaking features unless those features increase the orientational anisotropy of the system as a whole along the z-axis.

Although the coupling effects observed for the protein−water system (Figure 4A) generally agree with those observed for the water dimer system (Figure 5A), intermolecular couplings alone produce a larger effect in the protein−water system than in the model water dimer. It seems that the large effect of intermolecular couplings shown in Figure 4A may require water assemblies larger than a dimer or a shorter inter-water distance than assumed in the model system. The intramolecular couplings may also be somewhat inflated relative to the intermolecular couplings in this simple model because gas-phase values of mapped quantities are used. The intramolecular coupling in the gas phase is around −55 cm^{-1}, whereas the average value in bulk water is approximately −30 cm^{-1}.[36] We decided to use gas-phase values for the model system (i.e., ignore the electric field) to demonstrate that the effect of couplings is mainly a geometric or topological effect, rather than the result of emergent chirality in local fields. Local fields may still play a role in the real system, but they are not necessary for the coupling effect.

Intramolecular and intermolecular couplings can have synergistic effects. For the C_{3v} dimer system, intermolecular coupling alone produces a weaker signal than when all couplings are included even though intramolecular coupling alone produces no signal (Figure 5B). This observation suggests that intramolecular couplings contribute to the signal but only if allowed to do so by a symmetry-breaking feature such as intermolecular couplings. This effect is not seen in the methane (T_d) dimer (Figure 5C), suggesting that the synergistic effect of intramolecular and intermolecular couplings is system-dependent. Other symmetry-breaking features such as varying local electric fields may also be able to unlock chiral signals. However, all of our results suggest that intermolecular vibrational couplings alone are sufficient to unlock chiral signals in the simulated spectra.

The C_{2v} point group is effectively just asymmetric enough that the surviving hyperpolarizability components can give rise to a chiral SFG signal (eq 7). This is under the condition that the C_{2v} molecules are assembled in chiral supramolecular assemblies at an interface with C_∞ symmetry. Molecules of the C_{3v} point group, for example, have relatively higher symmetry, so all components of hyperpolarizability that can give rise to chiral signals disappear.[16] The same is true for other highly symmetric solvents. Although chiral SFG studies have focused on water interacting with biomolecules, our study suggests that any solvent surrounding a chiral solute at an interface with the C_∞ symmetry may be able to generate a chiral SFG signal provided that some symmetry-breaking features are present. Our results show that intermolecular vibrational couplings can be one of these features and generate chiral signals in simulated SFG spectra. This finding is consistent with the previously developed theory that predicts nonzero chiral 2D-SFG signals in pairs of achiral but coupled chromophores.[29]

The results in Figure 5B,C have significant implications for the study of the chiral SFG responses of nonaqueous solvents, some of which are highly symmetric molecules or contain highly symmetric functional groups, such as the -CCl_3 group in chloroform and methyl group in methanol. One of the most common chemical groups in organic solvents is the methyl group, which has C_{3v} symmetry. Figure 5B shows that a C_{3v} molecule (i.e., ammonia) can produce chiral SFG signals if heterogeneous intermolecular couplings are present. As the calculations in Figure 5 assume little about each chemical system except geometry and the presence of couplings, the results for one C_{3v} molecule translate qualitatively to all C_{3v} molecules and functional groups. Similarly, the results for methane translate qualitatively to tetrahedral solvents such as carbon tetrachloride. Accordingly, the symmetry-breaking feature of intermolecular (or more precisely, interfunctional group) couplings may explain the prominent chiral peak assigned to the methyl asymmetric stretch observed by Wang et al. in the antiparallel β-sheet $LK_7\beta$ peptides at the air−water interface.[45] Moreover, Geiger and co-workers observed a chiral SFG signal for methyl groups in DNA.[12,13] This observation has been a puzzle in the field because C_{3v} entities are forbidden to produce chiral SFG signals based on symmetry arguments. However, our results show that vibrational couplings or other environmental factors (e.g., local molecular interactions or electric fields) can potentially break the symmetry and induce chiral SFG signals.

In this study, we have discussed coupling between individual O−H vibrational modes. We found that coupling of some kind is essential to break the symmetry and allow for a chiral SFG signal. There are many vibrational modes, however, that involve symmetry-breaking coupling within the mode itself. This includes the amide I vibrational mode, which consists of both a carbonyl stretch and an N−H bend. In this case, intramolecular couplings are taken into account. Hence, it is not surprising that Skinner reports only a modest effect of intermolecular couplings of amide groups on the chiral SFG spectrum in the amide I region.[23]

Both the symmetric and asymmetric vibrational modes of water involve both O−H groups, but in isotopically labeled variants such as HOD, intramolecular coupling is minimal due to the difference in vibrational frequency of O−H (~3750 cm^{-1}) and O−D (~2750 cm^{-1}).[19,46] In this case, intramolecular coupling is ignored, and the symmetry-based theory predicts no chiral SFG signal. However, our results indicate that intermolecular couplings contribute substantially, and they alone can produce a basic lineshape that is similar to that for the combination of intramolecular and intermolecular couplings (Figure 4A). Hence, our simulations imply that

https://doi.org/10.1021/acs.jpcb.1c06360
J. Phys. Chem. B 2021, 125, 12072−12081

the O−H stretch in HOD systems surrounding chiral solutes will produce a chiral response. This is in agreement with isotope dilution experiments by Perets et al.[2]

CONCLUSIONS

This study examines the origin of the chiral SFG signal of the O−H stretch from aqueous interfaces containing chiral biomacromolecular solutes. Although vibrational couplings change the achiral SFG spectrum only slightly,[44] they are absolutely essential to the simulation of a chiral response. Our analysis indicates that vibrational couplings change the effective geometry of vibrational chromophores and introduce crucial asymmetry to induce chiral SFG responses. Our calculations show that the dependence on coupling arises even for a simple model system composed of two water molecules in a fixed geometry. Therefore, the effect of couplings on chiral SFG is not a phenomenon arising only in complex macromolecular systems.

Our findings have implications for theorists modeling SFG responses. Importantly, researchers using any method that omits vibrational couplings between O−H groups (or other bonds) must exercise caution when modeling chiral SFG signals. Intramolecular and intermolecular couplings are found to have comparable contributions to the chiral SFG response of water. Including intermolecular couplings as well as intramolecular couplings is not critical to qualitatively obtain a chiral response although it is necessary to obtain the full signal. In contrast, for molecules with higher symmetry than water, the symmetry-breaking effect of intermolecular couplings is absolutely required for the appearance of chiral SFG signals in the simulated spectra. Nonetheless, experimental detection of such signals depends on many factors (e.g., signal-to-noise level) and thus remains to be examined. Other symmetry-breaking effects, such as local molecular interactions and applications of external electric fields, may also be effective in inducing chiral SFG signals, and these remain to be explored with experiments and simulations. This study provides the foundation for investigating the solvation structure of synthetic chiral macromolecules in solvents other than water.

ASSOCIATED CONTENT

Supporting Information

The Supporting Information is available free of charge at https://pubs.acs.org/doi/10.1021/acs.jpcb.1c06360.

Additional discussion of some of the symmetry arguments, details of calculation of chiral SFG spectra from MD simulation trajectories, MD equilibration details, achiral (*ssp*) SFG response of water in terms of hyperpolarizability elements, details related to the model system calculations, and chiral SFG signal convergence information (PDF)

AUTHOR INFORMATION

Corresponding Authors

Elsa C. Y. Yan − *Department of Chemistry, Yale University, New Haven, Connecticut 06520, United States;* orcid.org/0000-0002-3583-1627; Email: elsa.yan@yale.edu

Sharon Hammes-Schiffer − *Department of Chemistry, Yale University, New Haven, Connecticut 06520, United States;* orcid.org/0000-0002-3782-6995; Email: sharon.hammes-schiffer@yale.edu

Authors

Daniel Konstantinovsky − *Department of Chemistry and Department of Molecular Biophysics and Biochemistry, Yale University, New Haven, Connecticut 06520, United States;* orcid.org/0000-0001-5718-7791

Ethan A. Perets − *Department of Chemistry, Yale University, New Haven, Connecticut 06520, United States;* orcid.org/0000-0001-9554-776X

Complete contact information is available at: https://pubs.acs.org/10.1021/acs.jpcb.1c06360

Notes

The authors declare no competing financial interest.

ACKNOWLEDGMENTS

The authors thank Dr. Pablo E. Videla at Yale University for insightful discussion. E.A.P. was supported by the NIH (5T32GM008283-31). D.K. was supported by the NIH (5T32GM008283-32). This work was supported by the National Institutes of Health Grant R35 GM139449 (S.H.-S.) and the NSF Grant CHE-2108690 (E.C.-Y.Y.).

REFERENCES

(1) McDermott, M. L.; Vanselous, H.; Corcelli, S. A.; Petersen, P. B. DNA's Chiral Spine of Hydration. *ACS Cent. Sci.* **2017**, *3*, 708−714.

(2) Perets, E. A.; Yan, E. C. Y. Chiral Water Superstructures around Antiparallel β-Sheets Observed by Chiral Vibrational Sum Frequency Generation Spectroscopy. *J. Phys. Chem. Lett.* **2019**, *10*, 3395−3401.

(3) Perets, E. A.; Yan, E. C. Y. The H2O Helix: The Chiral Water Superstructure Surrounding DNA. *ACS Cent. Sci.* **2017**, *3*, 683−685.

(4) Vanselous, H.; Petersen, P. B. Extending the capabilities of heterodyne-detected sum-frequency generation spectroscopy: probing any Interface in any polarization combination. *J. Phys. Chem. C* **2016**, *120*, 8175−8184.

(5) Perets, E. A.; Konstantinovsky, D.; Fu, L.; Chen, J.; Wang, H.-F.; Hammes-Schiffer, S.; Yan, E. C. Y. Mirror-image antiparallel β-sheets organize water molecules into superstructures of opposite chirality. *Proc. Natl. Acad. Sci. U. S. A.* **2020**, *117*, 32902−32909.

(6) Yan, E. C. Y.; Fu, L.; Wang, Z.; Liu, W. Biological Macromolecules at Interfaces Probed by Chiral Vibrational Sum Frequency Generation Spectroscopy. *Chem. Rev.* **2014**, *114*, 8471−8498.

(7) Wang, J.; Even, M. A.; Chen, X.; Schmaier, A. H.; Waite, J. H.; Chen, Z. Detection of Amide I Signals of Interfacial Proteins in Situ Using SFG. *J. Am. Chem. Soc.* **2003**, *125*, 9914−9915.

(8) Hosseinpour, S.; Roeters, S. J.; Bonn, M.; Peukert, W.; Woutersen, S.; Weidner, T. Structure and Dynamics of Interfacial Peptides and Proteins from Vibrational Sum-Frequency Generation Spectroscopy. *Chem. Rev.* **2020**, *120*, 3420−3465.

(9) Fu, L.; Liu, J.; Yan, E. C. Y. Chiral Sum Frequency Generation Spectroscopy for Characterizing Protein Secondary Structures at Interfaces. *J. Am. Chem. Soc.* **2011**, *133*, 8094−8097.

(10) Perets, E. A.; Videla, P. E.; Yan, E. C. Y.; Batista, V. S. Chiral inversion of amino acids in antiparallel beta sheets at interfaces probed by vibrational sum frequency generation spectroscopy. *J. Phys. Chem. B* **2019**, *123*, 5769−5781.

(11) Wurpel, G. W. H.; Sovago, M.; Bonn, M. Sensitive Probing of DNA Binding to a Cationic Lipid Monolayer. *J. Am. Chem. Soc.* **2007**, *129*, 8420−8421.

(12) Stokes, G. Y.; Gibbs-Davis, J. M.; Boman, F. C.; Stepp, B. R.; Condie, A. G.; Nguyen, S. T.; Geiger, F. M. Making "Sense" of DNA. *J. Am. Chem. Soc.* **2007**, *129*, 7492−7493.

(13) Walter, S. R.; Geiger, F. M. DNA on Stage: Showcasing Oligonucleotides at Surfaces and Interfaces with Second Harmonic and Vibrational Sum Frequency Generation. *J. Phys. Chem. Lett.* **2010**, *1*, 9−15.

(14) Tan, J.; Zhang, J.; Li, C.; Luo, Y.; Ye, S. Ultrafast energy relaxation dynamics of amide I vibrations coupled with protein-bound water molecules. *Nat. Commun.* **2019**, *10*, 1010.
(15) Fu, L.; Chen, S.-L.; Wang, H.-F. Validation of Spectra and Phase in Sub-1 cm−1 Resolution Sum-Frequency Generation Vibrational Spectroscopy through Internal Heterodyne Phase-Resolved Measurement. *J. Phys. Chem. B* **2016**, *120*, 1579−1589.
(16) Moad, A. J.; Simpson, G. J. A Unified Treatment of Selection Rules and Symmetry Relations for Sum-Frequency and Second Harmonic Spectroscopies. *J. Phys. Chem. B* **2004**, *108*, 3548−3562.
(17) Auer, B. M.; Skinner, J. L. Dynamical effects in line shapes for coupled chromophores: Time-averaging approximation. *J. Chem. Phys.* **2007**, *127*, No. 104105.
(18) Auer, B. M.; Skinner, J. L. Vibrational Sum-Frequency Spectroscopy of the Water Liquid/Vapor Interface. *J. Phys. Chem. B* **2009**, *113*, 4125−4130.
(19) Pieniazek, P. A.; Tainter, C. J.; Skinner, J. L. Interpretation of the water surface vibrational sum-frequency spectrum. *J. Chem. Phys.* **2011**, *135*, No. 044701.
(20) DeGrado, W. F.; Lear, J. D. Induction of peptide conformation at apolar water interfaces. 1. A study with model peptides of defined hydrophobic periodicity. *J. Am. Chem. Soc.* **1985**, *107*, 7684−7689.
(21) Morita, A.; Hynes, J. T. A Theoretical Analysis of the Sum Frequency Generation Spectrum of the Water Surface. II. Time-Dependent Approach. *J. Phys. Chem. B* **2002**, *106*, 673−685.
(22) Ohto, T.; Usui, K.; Hasegawa, T.; Bonn, M.; Nagata, Y. Toward ab initio molecular dynamics modeling for sum-frequency generation spectra; an efficient algorithm based on surface-specific velocity-velocity correlation function. *J. Chem. Phys.* **2015**, *143*, No. 124702.
(23) Carr, J. K.; Wang, L.; Roy, S.; Skinner, J. L. Theoretical Sum Frequency Generation Spectroscopy of Peptides. *J. Phys. Chem. B* **2015**, *119*, 8969−8983.
(24) Boyd, R. W., The Nonlinear Optical Susceptibility. In *Nonlinear Optics (Fourth Edition)*, Boyd, R. W., Ed. Academic Press: 2020, 1−64.
(25) Eisenthal, K. B. Liquid Interfaces Probed by Second-Harmonic and Sum-Frequency Spectroscopy. *Chem. Rev.* **1996**, *96*, 1343−1360.
(26) Richmond, G. L. Molecular Bonding and Interactions at Aqueous Surfaces as Probed by Vibrational Sum Frequency Spectroscopy. *Chem. Rev.* **2002**, *102*, 2693−2724.
(27) Shen, Y. R.; Ostroverkhov, V. Sum-Frequency Vibrational Spectroscopy on Water Interfaces: Polar Orientation of Water Molecules at Interfaces. *Chem. Rev.* **2006**, *106*, 1140−1154.
(28) Wang, H. F.; Gan, W.; Lu, R.; Rao, Y.; Wu, B. H. Quantitative spectral and orientational analysis in surface sum frequency generation vibrational spectroscopy (SFG-VS). *Int. Rev. Phys. Chem.* **2005**, *24*, 191−256.
(29) Laaser, J. E.; Zanni, M. T. Extracting Structural Information from the Polarization Dependence of One- and Two-Dimensional Sum Frequency Generation Spectra. *J. Phys. Chem. A* **2013**, *117*, 5875−5890.
(30) Horn, H. W.; Swope, W. C.; Pitera, J. W.; Madura, J. D.; Dick, T. J.; Hura, G. L.; Head-Gordon, T. Development of an improved four-site water model for biomolecular simulations: TIP4P-Ew. *J. Chem. Phys.* **2004**, *120*, 9665−9678.
(31) Maier, J. A.; Martinez, C.; Kasavajhala, K.; Wickstrom, L.; Hauser, K. E.; Simmerling, C. ff14SB: Improving the Accuracy of Protein Side Chain and Backbone Parameters from ff99SB. *J. Chem. Theory Comput.* **2015**, *11*, 3696−3713.
(32) Darden, T.; York, D.; Pedersen, L. Particle mesh Ewald: An N·log(N) method for Ewald sums in large systems. *J. Chem. Phys.* **1993**, *98*, 10089−10092.
(33) Miyamoto, S.; Kollman, P. A. Settle: An analytical version of the SHAKE and RATTLE algorithm for rigid water models. *J. Comput. Chem.* **1992**, *13*, 952−962.
(34) Ryckaert, J.-P.; Ciccotti, G.; Berendsen, H. J. C. Numerical integration of the cartesian equations of motion of a system with constraints: molecular dynamics of n-alkanes. *J. Comput. Phys.* **1977**, *23*, 327−341.
(35) Eastman, P.; Swails, J.; Chodera, J. D.; McGibbon, R. T.; Zhao, Y.; Beauchamp, K. A.; Wang, L.-P.; Simmonett, A. C.; Harrigan, M. P.; Stern, C. D.; Wiewiora, R. P.; Brooks, B. R.; Pande, V. S. OpenMM 7: Rapid development of high performance algorithms for molecular dynamics. *PLoS Comput. Biol.* **2017**, *13*, No. e1005659.
(36) Auer, B. M.; Skinner, J. L. IR and Raman spectra of liquid water: Theory and interpretation. *J. Chem. Phys.* **2008**, *128*, No. 224511.
(37) McGuire, J. A.; Shen, Y. R. Ultrafast Vibrational Dynamics at Water Interfaces. *Science* **2006**, *313*, 1945−1948.
(38) Belch, A. C.; Rice, S. A. The OH stretching spectrum of liquid water: A random network model interpretation. *J. Chem. Phys.* **1983**, *78*, 4817−4823.
(39) Michaud-Agrawal, N.; Denning, E. J.; Woolf, T. B.; Beckstein, O. MDAnalysis: A toolkit for the analysis of molecular dynamics simulations. *J. Comput. Chem.* **2011**, *32*, 2319−2327.
(40) Harris, C. R.; Millman, K. J.; van der Walt, S. J.; Gommers, R.; Virtanen, P.; Cournapeau, D.; Wieser, E.; Taylor, J.; Berg, S.; Smith, N. J.; et al. Array programming with NumPy. *Nature* **2020**, *585*, 357−362.
(41) Max, J.-J.; Chapados, C. Infrared spectroscopy of acetone-hexane liquid mixtures. *J. Chem. Phys.* **2007**, *126*, No. 154511.
(42) Scherer, J. R.; Snyder, R. G. Raman intensities of single crystal ice Ih. *J. Chem. Phys.* **1977**, *67*, 4794−4811.
(43) Kocsis, I.; Sorci, M.; Vanselous, H.; Murail, S.; Sanders, S. E.; Licsandru, E.; Legrand, Y.-M.; van der Lee, A.; Baaden, M.; Petersen, P. B.; et al. Oriented chiral water wires in artificial transmembrane channels. *Sci. Adv.* **2018**, *4*, No. eaao5603.
(44) Kaliannan, N. K.; Henao Aristizabal, A.; Wiebeler, H.; Zysk, F.; Ohto, T.; Nagata, Y.; Kühne, T. D. Impact of intermolecular vibrational coupling effects on the sum-frequency generation spectra of the water/air interface. *Mol. Phys.* **2020**, *118*, No. 1620358.
(45) Wang, Z.; Fu, L.; Yan, E. C. Y. C−H Stretch for Probing Kinetics of Self-Assembly into Macromolecular Chiral Structures at Interfaces by Chiral Sum Frequency Generation Spectroscopy. *Langmuir* **2013**, *29*, 4077−4083.
(46) Wiafe-Akenten, J.; Bansil, R. Intermolecular coupling in HOD solutions. *J. Chem. Phys.* **1983**, *78*, 7132−7137.

NOTE ADDED AFTER ASAP PUBLICATION

This paper published ASAP on October 26, 2021 with an error in eq (8). The corrected version reposted with the issue on November 4, 2021.

https://doi.org/10.1021/acs.jpcb.1c06360
J. Phys. Chem. B 2021, 125, 12072−12081